

# <sup>3</sup> Single-molecule stretching shows glycosylation sets <sup>4</sup> tension in the hyaluronan-aggrecan bottlebrush

<sup>5</sup> S. N. Innes-Gold<sup>1</sup>, J. P. Berezney<sup>1,†</sup>, and O. A. Saleh<sup>1,2,\*</sup>

<sup>6</sup> <sup>1</sup>University of California, Santa Barbara, Materials Department

<sup>7</sup> <sup>2</sup>University of California, Santa Barbara, Biomolecular Science and Engineering Program

<sup>8</sup> <sup>†</sup>Current affiliation: Brandeis University, Physics Department

<sup>9</sup> <sup>\*</sup>Correspondence: saleh@ucsb.edu

**10 ABSTRACT** Large bottlebrush complexes formed from the polysaccharide hyaluronan (HA) and the proteoglycan aggrecan contribute to cartilage compression resistance and are necessary for healthy joint function. A variety of mechanical forces act on these complexes in the cartilage extracellular matrix, motivating the need for a quantitative description which links their structure and mechanical response. Studies using electron microscopy have imaged the HA-aggrecan brush but require adsorption to a surface, dramatically altering the complex from its native conformation. We use magnetic tweezers force spectroscopy to measure changes in extension and mechanical response of an HA chain as aggrecan monomers bind and form a bottlebrush. This technique directly measures changes undergone by a single complex with time and under varying solution conditions. Upon addition of aggrecan, we find a large swelling effect manifests when the HA chain is under very low external tension (i.e. stretching forces less than  $\sim 1$  pN). We use models of force-extension behavior to show that repulsion between the aggrecans induces an internal tension in the HA chain. Through reference to theories of bottlebrush polymer behavior, we demonstrate that the experimental values of internal tension are consistent with a polydisperse aggrecan population, likely caused by varying degrees of glycosylation. By enzymatically deglycosylating aggrecan, we show that aggrecan glycosylation is the structural feature which causes HA stiffening. We then construct a simple stochastic binding model to show that variable glycosylation leads to a wide distribution of internal tensions in HA, causing variations in the mechanics at much longer length-scales. Our results provide a mechanistic picture of how flexibility and size of HA and aggrecan lead to the brush architecture and mechanical properties of this important component of cartilage.

**26 SIGNIFICANCE** We use single-molecule stretching experiments to study a macromolecular complex of hyaluronan and aggrecan whose structure is crucial to maintaining mechanical strength of articular cartilage. We experimentally validate a model which quantitatively describes how the extension of an HA chain is affected by binding aggrecan side chains. This model yields information about the sensitivity of the complex size to different features of the bottlebrush architecture, and predicts when and how aggrecan damage leads to collapse of the complex.

## **27 INTRODUCTION**

**28** Large bottlebrush complexes formed from the polysaccharide hyaluronan (HA) and the proteoglycan aggrecan constitute a major component of cartilage (1). HA is a long, linear polyelectrolyte with a charge density of  $1\text{ e/nm}$ , a persistence length of around  $5\text{ nm}$ , and a native size of  $\sim 1\text{-}10\text{ MDa}$ , corresponding to contour lengths of  $\sim 2\text{-}20\text{ }\mu\text{m}$  (2). In cartilage, HA is secreted by chondrocytes and anchored to the cell surface by HA synthases or the receptor CD44 (3), forming the sugar-rich “glycocalyx” coating around the cell. Each HA chain in the glycocalyx is complexed with many non-covalently bound aggrecans to form a large macromolecular bottlebrush that is known to be a major contributor to cartilage compression resistance (4). In cartilage, the complex involves a third participant, link protein (LP), which binds to both HA and aggrecan to stabilize the interaction (4). As illustrated in Fig. 1A, each aggrecan monomer is itself a bottlebrush, consisting of a  $\sim 300\text{ kDa}$  protein core which is densely decorated by the glycosaminoglycan side chains keratan sulfate (KS) and the more abundant chondroitin sulfate (CS) (4). The core protein includes three globular domains: two at the N-terminus (G1 and G2) and one at the C-terminus (G3) (1). G1 is the HA-binding domain. In between G2 and G3 is an extended domain decorated by  $\sim 100$  CS chains (1). The high charge and large size of aggrecan result primarily from this CS-rich region. This structure-defining domain changes with age, showing a reduction in the number and size of CS side chains (5–10).

**41** Previous studies have used electron microscopy and atomic force microscopy (AFM) to visualize the structure of individual aggrecans and aggrecan-HA complexes (10–14). These studies have provided estimates of the length and diameter of aggrecan, as well as the density of bound aggrecans on an HA chain. However, imaging requires adsorption to a surface which significantly distorts the conformation of the complex. In order to learn about the solution structure of the complex, including the conformation adopted by the central HA chain, it is necessary to probe the structure of individual complexes by a method that does not confine the aggregates to 2D. To this end, others have used single-molecule force spectroscopy to measure properties of the complexes, such as inter-aggrecan interactions (15, 16). AFM and laser tweezers, which can access forces on the order of 10–1000 and 1–100 pN respectively (17, 18), have also been used to test the strength of the bond connecting aggrecan and HA (19–22). Liu *et. al.* used laser tweezers to probe moderate-force tensile behavior ( $\sim 10\text{-}40\text{ pN}$ ) and compressibility of single HA-aggrecan complexes (23, 24).

**51** To our knowledge, no prior work has conducted low-force tensile testing on single bottlebrush complexes with sub-piconewton resolution, despite this likely being the biologically relevant force range: a study on osteocytes estimated that flow forces can lead to tension in the cell-attached components (e.g. HA) in the range of  $\sim 1\text{-}10\text{ pN}$  (25). Here, we aim to quantify the structure of the complex based on its response to forces in this range. To do this, we use magnetic tweezers force spectroscopy. Prior work has shown that magnetic tweezers are particularly useful for quantifying structural changes that manifest at low forces, such as intra-chain electrostatic repulsion (26). Thermally dominated structure at a particular length-scale  $x$  is probed by forces of the scale  $k_B T/x$  (18, 27). Magnetic tweezers typically apply forces on the order of 0.01–10 pN, and thus are sensitive

58 to structure on length-scales between  $\sim$ 1-100s of nm. Because of this long length-scale sensitivity, magnetic tweezers have  
 59 succeeded in measuring the structural changes induced by side chains in a synthetic polymer bottlebrush (28).

60 By applying low-force magnetic tweezers stretching to study the formation and properties of the HA-aggrecan bottlebrush  
 61 complex, we arrive at a novel physical description of this important component of cartilage. Prior work has shown that aggrecan  
 62 swells HA chains in pericellular coats (33) and pure HA brushes (34); we find this effect is also detectable at the single-chain  
 63 level. Thus, we can observe in real time the assembly of the complexes by tracking the increase in chain extension. We find our  
 64 data are well-described by a model in which the effect of all inter-aggrecan repulsions can be combined into a single internal  
 65 tension, which acts in combination with the externally applied stretching force to extend the HA chain. We show that, on  
 66 average, the internal tension generated in the central HA chain is about 0.4 pN, but with large variability between measurements.  
 67 We use an analytical theory of bottlebrush physics to show that the spread in the data is consistent with variability in degree of  
 68 glycosylation of the bound aggrecan.

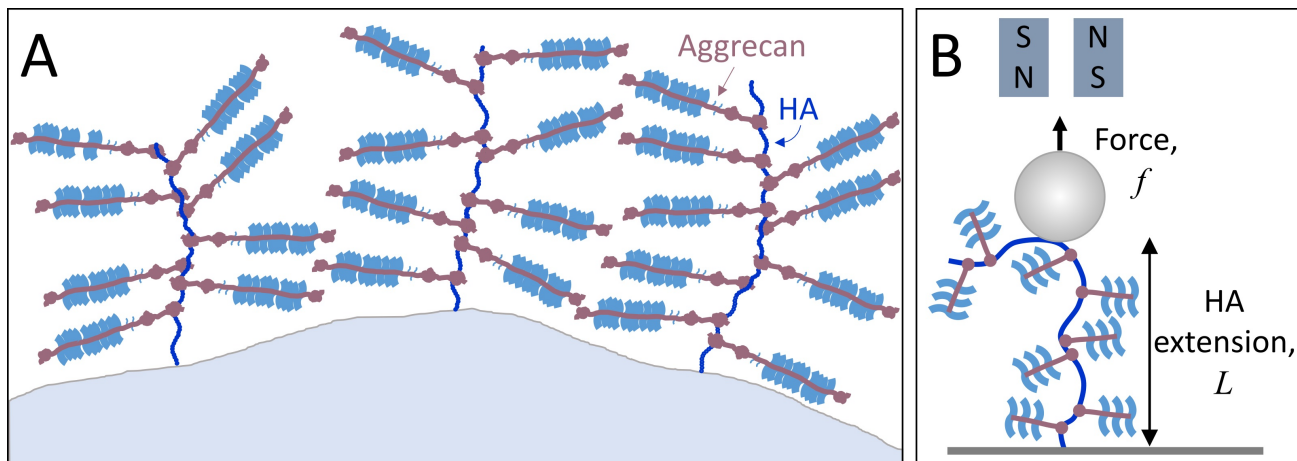


Figure 1: A. Cartoon of the chondrocyte glycocalyx, wherein HA chains are tethered to the cell surface and decorated with the proteoglycan aggrecan, forming a microns-thick coating around the cell. B. Experimental set-up: a single HA chain, decorated by aggrecans, is tethered between a glass surface and a magnetic bead. A magnet applies stretching forces to the HA chain at the center of the bottlebrush.

## 69 MATERIALS AND METHODS

70 Hyaluronic acid (2.5 MDa), chemically functionalized to allow tethering to two surfaces, was purchased from Creative  
 71 PEGworks. Each HA chain has a biotin group at the reducing end, and randomly situated thiol groups with a stoichiometry  
 72 of one thiol per chain. Microfluidic sample chambers were constructed using maleimide-functionalized PEG-grafted glass  
 73 coverslips purchased from Microsurfaces, Inc. HA chains were attached to the surface via reaction of the thiol groups with  
 74 the maleimide, carried out in 50 mM sodium phosphate buffer (pH 7.2), 50 mM NaCl, 0.03% Tween-20, and 100 mM TCEP.  
 75 After attachment, excess polymer was removed by rinsing with 10 mM MOPS buffer (pH 7, with ionic strength of 4 mM).  
 76 Streptavidin-coated magnetic beads, 1  $\mu$ m in diameter (MyOne C1 paramagnetic beads, Invitrogen) were attached to the  
 77 biotin-labeled chain ends.

78 This experimental protocol leads to polydispersity in the tether lengths due to the random locations of the thiols, and  
 79 necessitates normalization by contour length to compare measurements on different tethers. We expect an approximately  
 80 uniform distribution of tether sizes up to  $\sim$ 6  $\mu$ m. However, due to the potential for bead-surface interactions at low forces, we  
 81 do not collect data on tethers shorter than  $\sim$ 0.6  $\mu$ m. The stochastic thiol labeling strategy means that the magnetic bead is  
 82 attached internally within the chain, and thus that there is a second aggrecan-decorated HA (not pinned to the surface, and so  
 83 under no tension) in close proximity to the elastically-tested tether (see Fig. 1B). The excluded volume presented by this second  
 84 chain is small compared to the bead and surface, and we do not expect it to have an effect at the forces probed here.

85 Aggrecan ( $\geq$ 2.5 MDa, purified from bovine articular cartilage) was purchased from Sigma-Aldrich. It was centrifuged  
 86 to remove large aggregates, and small contaminants were removed by filtration with a 100 kDa spin column. Recombinant  
 87 aggrecan G1-IGD-G2 (with C-terminal 10-His tag) was purchased from Biolegend. Experiments were conducted in 100 mM  
 88 NaCl, 1-10 mM MOPS (pH 7), and 0.03% Tween-20.

89 Experiments were conducted using a custom-built magnetic tweezers instrument, as described in detail elsewhere (31).

90 Briefly, HA-tethered beads are imaged, and bead position is measured using an image analysis routine based on the bead's  
 91 diffraction pattern. The output of that routine includes the tether length and lateral bead fluctuations; the latter are analyzed to  
 92 estimate the applied tension (32). To ensure each bead is tethered by a single HA chain, the tether length is measured as the  
 93 bead is rotated. Multiple tethers become interwound during rotation, leading to a characteristic decrease in bead height (29).

94 Experiments on aggrecan-induced swelling used an aggrecan concentration of 2 mg/mL (approximately 0.8  $\mu$ M). Above ~1  
 95 mg/mL, the HA chain extension does not change appreciably with additional aggrecan (Fig. S1). A concentration of 2 mg/mL is  
 96 well into the concentration insensitive regime, and is close to the overlap concentration at which the distance between aggrecans  
 97 in solution approaches the aggrecan radius of gyration (35). This relatively high solution concentration is still well below the  
 98 density of aggrecan bound in cartilage, thought to be on the order of 10s of mg/mL (30). For experiments using the G1-IGD-G2  
 99 fragment, the protein was dissolved at ~0.8  $\mu$ M.

100 To obtain deglycosylated aggrecan core protein, aggrecan (Sigma-Aldrich) was incubated overnight with chondroitinase  
 101 ABC (Recombinant *P. vulgaris* Chondroitinase ABC with N-terminal Met and 6-His tag, purchased from R&D Systems). The  
 102 reaction took place at 37°C in 50 mM Trizma HCl (pH 8), 60 mM sodium acetate, 0.02% BSA. Chondroitinase ABC digests  
 103 HA in addition to chondroitin sulfate, so it was necessary to separate it from the deglycosylated aggrecan before experiments  
 104 could proceed. Separation was accomplished using Dynabeads His-Tag Isolation and Pulldown, which were then removed  
 105 magnetically. The presence of aggrecan core protein (~300 kDa) at the expected concentration was confirmed with SDS-PAGE  
 106 (Supplement, Fig. S2) and Dynamic Light Scattering on denatured aggrecan (Fig. S3) using a Malvern Zetasizer Nano ZS  
 107 instrument. HA force-extension curves in the presence of aggrecan core protein were obtained in 100 mM NaCl, 10 mM  
 108 MOPS (pH 7), 0.03% Tween-20, and 1 mg/mL free chondroitin sulfate (chondroitin sulfate sodium salt from shark cartilage,  
 109 purchased from Sigma-Aldrich). The free chondroitin sulfate was included in order to protect the HA tethers from digestion by  
 110 any residual enzyme, and was shown to have no effect on the HA mechanical response (Supplement, Fig. S4).

## 111 RESULTS

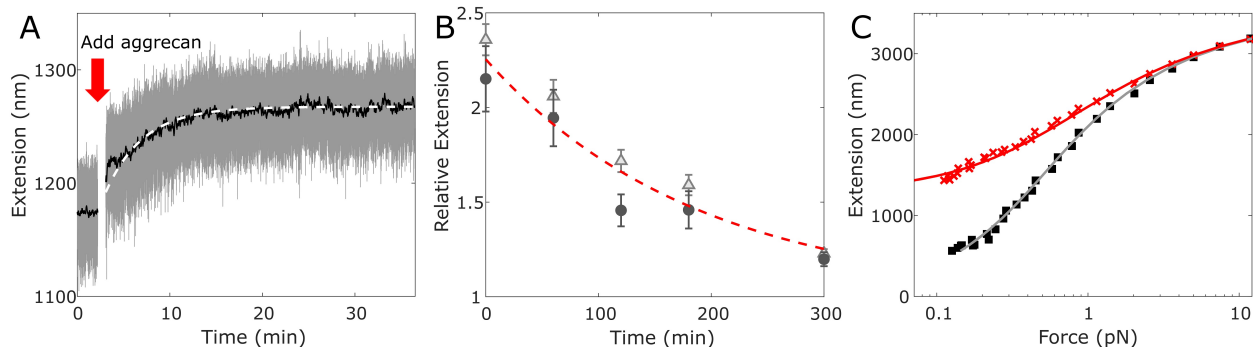


Figure 2: A. HA extension while aggrecan binds (gray: all points; black: moving average over 4 seconds) under a constant applied force of 1.8 pN. The data are fit by an exponential with a characteristic timescale of  $244 \pm 2$  seconds (white dashed line). B. HA extension during aggrecan unbinding. After removing free aggrecan from the bulk solution, extension of two aggrecan-decorated tethers at 0.2 pN (first tether: light gray triangles, second tether: dark gray circles), relative to aggrecan-free extension of the same tether at the same force, slowly decreases towards 1. Error bars show uncertainty arising from interpolation of force-extension curves at 0.2 pN. The data are fit by an exponential with a characteristic timescale of  $190 \pm 50$  minutes (red dashed line). C. Example force-extension data on a single HA tether before (black squares) and after (red x's) addition of 2 mg/mL aggrecan and equilibration of at least 15 minutes. Both force-extension curves are globally fit by Eq. 1, with common contour length  $L_C$  and persistence length  $l_p$ . Best-fit parameters are  $L_C = 3573 \pm 14$  nm,  $l_p = 7.4 \pm 0.4$  nm, and  $f_{int} = 0.40 \pm 0.03$  pN, where  $f_{int}$  is the internal tension generated by aggrecan ( $f_{int}$  is set to zero for the data measured without aggrecan). Errors reflect 95% confidence intervals for the fit parameters.

112 With magnetic tweezers, we measure the extension of tethered HA chains as aggrecan is added to solution. Our data show  
 113 that aggrecan expands the HA chain upon binding (Fig. 2). When the chain is minimally stretched, we can track the progress of  
 114 aggrecan binding by monitoring the chain end-to-end extension. As can be seen in Fig. 2A, the length increases upon addition of  
 115 2 mg/mL aggrecan, and levels off after about 15 minutes, indicating the system has equilibrated. We can subsequently rinse free  
 116 aggrecan out of the bulk solution and observe the HA length change as aggrecan unbinds (Fig. 2B). This process takes several  
 117 hours. Comparing timescales obtained by fitting exponential models to the data, we estimate that the timescale of aggrecan

binding is at least 50 times faster than aggrecan unbinding. While aggrecan interactions may lead to anti-cooperative behavior and non-exponential kinetics, the data (within the experimental resolution) appear exponential. Thus, to good approximation, a simple independent binding picture can be used, which here indicates that, since the off-rate is 50x slower than the on-rate, the maximal aggrecan density on HA has been achieved. We note that in cartilage, link protein would further stabilize the bound state, likely causing higher aggrecan density and even slower unbinding.

Relative to the mechanical behavior measured before the addition of aggrecan, the ligand-binding dramatically alters the low-force response (see example data in Fig. 2C). Repeated experiments on 10 HA tethers, with and without aggrecan, all show similar elasticity changes (Fig. 3). With the addition of aggrecan (2 mg/mL), all tethers undergo swelling at low forces; this is reflected by the shallower slopes of the force-extension curves. The slope change indicates that aggrecan binding stiffens the chain, causing it to become less responsive to the externally-applied force. The observed low-force elasticity change is consistent with long length-scale structural effects: swelling and stiffening of the central HA chain due to repulsion between bound aggrecans, as expected from the charged brush structure of the aggrecan monomers (36).

We quantify the low-force swelling using an internal tension model (26), in which the long length-scale stiffening (caused by the bottlebrush architecture) is described by a mean-field internal tension  $f_{int}$ , which acts in addition to the applied force  $f$  to straighten the polymer. This first-order correction captures the deviation from wormlike chain elasticity, which is most prominent at low forces where the chain physics is dominated by long-range side-chain interactions. The internal tension term is incorporated into the Marko-Siggia wormlike chain (WLC) model (37), giving:

$$f = \frac{k_B T}{l_p} \left( \frac{1}{4} \left( 1 - \frac{L}{L_C} \right)^{-2} - \frac{1}{4} + \frac{L}{L_C} \right) - f_{int} \quad (1)$$

where  $l_p$  is the intrinsic HA persistence length,  $L$  is the chain extension, and  $L_C$  is the contour length. Eq. 1 is used to fit force-extension data, with  $L_C$  and  $l_p$  fit globally for pairs of curves on the same molecule.  $f_{int}$  is fixed to zero for the bare HA force-extension data (example: Fig. 2C). We repeated such analyses on each of the ten tethers, measuring force-extension curves before and after the addition of 2 mg/mL aggrecan, and extracting  $f_{int}$  as a fit parameter. The average was  $0.35 \pm 0.21$  pN (standard deviation). The spread in  $f_{int}$  reflects variability in the response of the aggrecan-decorated chains, demonstrated by the scatter of the red traces in Fig. 3. We hypothesize that this variability arises due to differences in glycosylation of the aggrecan samples, which originated in biological tissue (7, 38, 39).

For comparison, we digested the CS side chains of the aggrecan using chondroitinase ABC, and found that the resulting deglycosylated protein induces almost no swelling in HA (blue lines in Fig. 3). While the less abundant KS side chains are thought not to be affected by this enzyme, others have shown that in contrast to CS, removal of the KS side chains has little to no effect on the aggrecan monomer structure (5).

## DISCUSSION

The HA-aggrecan force-extension data highlight that properties of the side chains play a crucial role in defining the bottlebrush architecture. At low forces ( $\sim 0.1$  pN), the end-to-end extension of HA molecules often increases more than twofold upon introduction of aggrecan. However, when HA is decorated instead by deglycosylated aggrecan, this bottlebrush-induced stiffening is dramatically reduced, demonstrating the importance of the chemical details of aggrecan. Even without artificial reduction of aggrecan glycosylation, the experiments display a wide range of responses. These observations can be explained using established polymer bottlebrush theory. We show the full range of stiffening observed is consistent with predictions from scaling theory combined with previous experimental measurements of HA and aggrecan structure. We further find that the variance in the glycosylated aggrecan data is consistent with an aggrecan population of varying degrees of glycosylation. Such results demonstrate the interplay between the branched architecture of the complex and the conformational structure of its constituent chains.

Following the logic of Berezney *et. al.* (28), we use a model developed by Panyukov *et. al.* (40) to predict, independently of our own measurements, the range of internal tensions in the HA backbone of bottlebrush complexes extended by glycosylated and deglycosylated aggrecan. The model treats the side chains as random walk polymers whose size, flexibility, and binding density control the internal tension generated in the central chain:

$$f_{int} = \alpha k_B T d^\mu b_a^{-(\mu+1)} n^\nu |\tau|^t \quad (2)$$

where  $\alpha$  is a prefactor that we take to be 1,  $\mu$ ,  $\nu$ , and  $t$  are scaling exponents (described below),  $b_a$  is the statistical segment length of aggrecan,  $n$  is the number of statistical segments within each aggrecan side chain,  $\tau$  describes solvent quality and is 1 in good solvent, and  $d$  is the distance between bound aggrecans. Estimates of  $d$  range from 12-40 nm (13, 14); we choose the intermediate value of this range: 26 nm. If link protein were present, a smaller value ( $\sim 10$  nm) would be appropriate as link

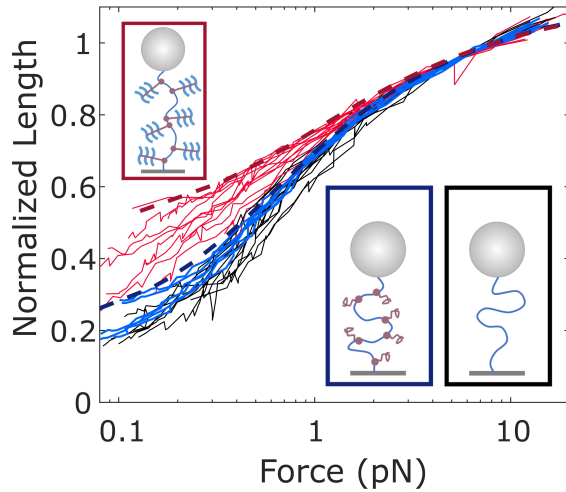


Figure 3: Thin red lines show force-extension curves on 10 HA tethers with 2 mg/mL aggrecan. Extensions are normalized by multiplicative adjustment, with factors determined by comparing each curve to the median of the ten, and minimizing the sum of squared residuals in length for forces between 3 and 10 pN. Black lines show force-extension curves on the same 10 tethers in aggrecan-free conditions. Blue lines show force-extension curves of 6 HA tethers in the presence of deglycosylated aggrecan core protein. Thick dashed lines are predictions from the WLC-internal tension model for fully glycosylated aggrecan (dark red) and aggrecan core protein (dark blue). Cartoons (inset) illustrate the conditions for each set of force-extension curves (full aggrecan: red box, upper left; chABC-digested aggrecan: blue box, bottom middle; bare HA: black box, bottom right).

protein is known to increase aggrecan density (13). Based on our experiments showing unbinding is very slow, we assume the number and spacing of bound aggrecans are constant over experimental timescales (measurement of each force-extension curve takes 20 minutes). We assume that deglycosylation will be reflected as a change in aggrecan's Kuhn length  $b_a$ . The model (Eq. 2) considers the athermal limit and takes the excluded volume to be  $b_a^3$ . For bottlebrushes, Kuhn length typically scales with the diameter of the complex (41). Thus for fully glycosylated aggrecan, we will approximate  $b_a \approx 50$  nm, roughly the diameter of the cylindrical proteoglycan (14). In the opposite limit of complete deglycosylation, the side chains are aggrecan core protein alone. Based on the disordered nature of much of the core protein (42), we estimate  $b_a$  as 1.6 nm, twice the persistence length of an unfolded polypeptide (43). This value represents a physical lower limit; in reality it is likely that some residual structure leads to a slightly larger Kuhn length (42), but the model is not very sensitive to this assumption (Fig. S6). The number of segments  $n$  is obtained by dividing the aggrecan contour length, estimated as 375 nm following AFM studies, (10, 14) by the Kuhn length. SDS-PAGE of the deglycosylated protein (Fig. S2) shows a number of bands near the expected weight, suggesting there may be a spread of aggrecan sizes present; we do not incorporate this into our model but recognize that it may be an additional source of variability.

We assume the central HA chain is always strongly stretched due to its stiffness ( $b_{HA} \approx 10$  nm), side chains, and the external force, thus, the random coil structure of the side chains will be the dominant contributor to the HA internal tension. It is expected that deglycosylation will significantly perturb aggrecan structure; this will change not only its Kuhn length as discussed above, but also the scaling laws describing its solution structure. Fully-glycosylated aggrecan is strongly extended due to repulsion between its own CS branches. Following Panyukov *et. al.* (40), the case of swollen aggrecan side chains dictates  $\mu = -13/8$ ,  $\nu = 3/8$ , and  $t = 1/8$  in Eq. 2.

The deglycosylated core protein structure will also likely be dominated by the large CS-attachment region, now devoid of CS. Prior evidence has shown that the CS-attachment domain of aggrecan is structurally disordered (42). The solution structure of intrinsically disordered proteins reflects a trade off between conformational flexibility and transient short length-scale interactions, and is frequently modeled by ideal scaling (44). Thus, we assume that without CS to provide stretching, the core protein will behave ideally, dictating scaling exponents  $\mu = -5/3$ ,  $\nu = 1/3$ , and  $t = 0$ . We note that the model of Panyukov *et. al.* is formally correct for a bottlebrush whose backbone and side chains have the same chemistry, which is not the case here. However, as discussed above, HA elasticity is not expected to have significant effects because the chain is always in a regime of strong stretching. Further, if we instead assume the core protein is swollen, the predicted tension does not change drastically (Fig. S6).

This model (Eq. 2 with parameters listed above) allows us to estimate the range of  $f_{int}$  values expected for aggrecan in

194 different conditions: 0.15 pN in the limit of complete deglycosylation, and 0.51 pN for a monodisperse sample of undamaged  
 195 aggrecan. Combining these values with the WLC model (Eq. 1), we obtain expected force-extension curves for HA decorated  
 196 by whole aggrecan (dark red dashed curve in Fig. 3) and HA decorated by deglycosylated aggrecan core protein (dark blue  
 197 dashed curve in Fig. 3). Our experimental force-extension curves for aggrecan-decorated HA (Fig. 3) mostly fall between these  
 198 limits, where the experimental curves showing the largest swelling are consistent with the undamaged aggrecan prediction  
 199 of  $f_{int} \approx 0.5$  pN. The force-extension curves on HA with deglycosylated aggrecan core protein (blue traces in Fig. 3) nearly  
 200 coincide with the model's prediction for deglycosylated aggrecan. As noted above, in cartilage the complex is often stabilized  
 201 by link protein, which reduces the aggrecan spacing to  $d \approx 10$  nm. As  $f_{int}$  depends sensitively on  $d$ , link protein's contribution  
 202 will likely lead to a much higher tension in healthy physiological complexes:  $\sim 2$  pN, instead of  $\sim 0.5$  pN as reported here.

### 203 Aggrecan polydispersity

204 The above model makes predictions for extreme cases: monodisperse populations of either undamaged aggrecan or completely  
 205 deglycosylated core protein. It is clear that a monodisperse population of aggrecan with intermediate glycosylation (and thus  $b_a$   
 206 between 1.6 nm and 50 nm) would generate a tension intermediate between these cases. In practice however, there will usually  
 207 be a mixture of aggrecan at varying levels of glycosylation, ranging from the bare core protein to a dense bottlebrush. In the  
 208 following, we consider a two-species mixture of undamaged and deglycosylated aggrecan. In neglecting intermediate levels of  
 209 glycosylation, this scenario is still a significant simplification. Nonetheless, it illustrates how polydispersity in the aggrecan  
 210 population can lead to variability in the extension of aggrecan-decorated HA chains.

211 We consider a simple model where the HA chain is represented by a 1D array of binding sites, spaced by  $d = 26$  nm. Each  
 212 site can be occupied either by an undamaged aggrecan (A) or a deglycosylated core protein (B). Each bound side chain interacts  
 213 only with its nearest neighbors, stretching the intervening HA segment. If stretched by A's, the segment will experience  $f_{int}^{AA} =$   
 214 0.51 pN, as calculated above, while a segment stretched by two B's will experience  $f_{int}^{BB} = 0.15$  pN. We assume that the tension  
 215 in a segment with one A neighbor and one B neighbor,  $f_{int}^{AB}$ , is closer to the completely deglycosylated case due to the lack of  
 216 charged CS on the core protein, as well as its presumed ideal (i.e. self-intersecting) behavior. Thus we take  $f_{int}^{AB} = 0.15$  pN as  
 217 well. We define  $\Phi$  as the fraction of undamaged A aggrecan in the bulk solution, and populate each binding site stochastically  
 218 with probability  $P(A) = \Phi$ . We use the asymptotic form of the MS-WLC expression (37) to predict the relative length of a  
 219 segment as a function of the total force it experiences (external force + internal tension):

$$\frac{L_{seg}^{seg}}{L_c^{seg}} = 1 - \sqrt{\frac{k_B T}{4(f + f_{int})l_p}}. \quad (3)$$

220 We count the number of each type of segment (A-A, A-B, and B-B) to approximate force-extension curves for HA decorated by  
 221 a heterogeneous aggrecan population.

222 In our model, variability can arise due to two factors. The quality of aggrecan may differ between samples; thus we make  $\Phi$   
 223 a random variable. We will set the mean  $\bar{\Phi} = 0.8$ , and assume  $\Phi$  is normally distributed with a standard deviation of 10%.  
 224 Additionally, even without noise in  $\Phi$ , the randomness inherent in the binding process leads to fluctuations in the *actual* fraction  
 225 of A aggrecans bound, as well as their arrangement on the chain. For short HA tethers (e.g.  $\sim 600$  nm, or  $\sim 20$  binding sites),  
 226 these fluctuations from the average are significant. Our experimental setup invariably leads to polydispersity in tether length:  
 227 the tethers included in Fig. 3 range in length from  $\sim 600$  nm to  $\sim 5000$  nm ( $\sim 200$  binding sites). Thus, in our model, we select a  
 228 contour length at random from the set of 10 experimentally measured tethers.

229 Our model results qualitatively show that sample-to-sample variation in aggrecan quality, along with random fluctuations in  
 230 the actual bound population and arrangement on short tethers, can lead to the kind of noisy data we observe experimentally.  
 231 We simulate  $10^5$  tethers, each with random  $\Phi$  and  $L_c$  as described above. Force-extension curves for the first 10 trials are  
 232 plotted on the right side of Fig. 4. The histogram on the left of Fig. 4 shows the low-force (0.1 pN) extension of all  $10^5$   
 233 tethers. With no sample-to-sample variation ( $\Phi$  fixed to 0.8), this distribution narrows significantly, suggesting that sample  
 234 quality variation is needed to explain the data. Further, our experiments include two pairs of curves from tethers that were  
 235 measured simultaneously and thus experienced the same aggrecan sample (same  $\Phi$ ). These pairs of tethers show nearly identical  
 236 mechanical responses (Fig. S5), suggesting that sample-to-sample differences in aggrecan quality are the major cause of the  
 237 variability in the force-extension curves.

### 238 HA structure on short length-scales

239 Prior work has shown that some HA-binding proteins, such as the proteoglycan versican G1, bind cooperatively and may induce  
 240 higher-order helical structure in HA (45). Such a structure would affect the HA chain on relatively short length-scales, and  
 241 would be measured as a decrease in extension under relatively high tension. It is known that the aggrecan G1 domain binds to 5

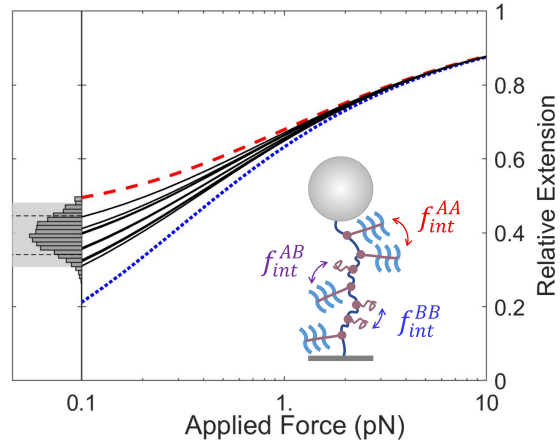


Figure 4: Predicted force-extension curves for HA in a mixture of undamaged and deglycosylated aggrecan. Right: Red dashed (blue dotted) curve shows the predicted force-extension behavior for  $\Phi = 1$  (0). Black curves show predicted force-extension for 10 tethers, each populated randomly with whole aggrecan and deglycosylated core protein according to probability  $\Phi$ , with  $\Phi$  drawn from a distribution of mean  $\bar{\Phi} = 0.8$ . For each tether,  $L_c$  is selected randomly as described in the text. Left: histogram shows the length at 0.1 pN for 100000 simulated tethers. The shaded gray region includes 95% of the data. The dashed lines indicate how this region would narrow if there were no noise in  $\Phi$ . Inset: schematic illustrating the 1D binding model and the heterogeneous tensions induced in segments throughout the chain.

242 disaccharide units (46), approximately equal to the intrinsic HA persistence length. Bends on this length-scale would likely  
 243 manifest as a decrease in the fit persistence length (47).

244 We see no evidence that aggrecan binding alters the short length-scale structure of HA by inducing bends or helical  
 245 superstructure. At sufficiently high force (significantly greater than  $\sim 1$  pN, probing structural features smaller than  $l_p$ ) we see  
 246 no difference between force-extension curves with and without aggrecan (example: Fig. 2C). Further, in agreement with Liu et.  
 247 al. (21), if we perform fits with persistence length as a free parameter, we do not find a statistically significant difference in  
 248 fit HA persistence length with and without aggrecan when swelling is accounted for by an internal tension (bare HA:  $l_p =$   
 249  $6.6 \pm 0.4$  nm; with aggrecan:  $l_p = 6.1 \pm 0.7$  nm,  $N = 10$ , reported errors are standard error of the mean). We note that these  
 250 estimates of the HA persistence length are consistent with prior magnetic tweezers experiments (28), but are systematically  
 251 larger than estimates from AFM (22); we attribute this to the general principle that high-tension stretching systematically biases  
 252 measurements to lower persistence lengths (48), e.g. by force disrupting local interactions and secondary structure in the chain.

253 To confirm this, we performed experiments using an HA-binding aggrecan fragment, G1-IGD-G2, which lacks the large  
 254 CS-rich region that constitutes most of aggrecan's size and charge and is responsible for the large degree of swelling. Over the  
 255 range of forces which probe short length-scale structure, there is no discernible difference in the response with and without  
 256 G1-IGD-G2 (see example data in Fig. S7). Using SDS-PAGE, we qualitatively confirmed the fragment can bind to HA (Fig. S8).  
 257 These results are in agreement with others who have found that unlike versican G1, aggrecan G1 does not bind cooperatively,  
 258 does not pack tightly on HA, and does not cause the same superstructures (49). In vivo, aggrecan binds HA alongside link  
 259 protein in a ternary complex (4). It remains a possibility that link protein could induce higher-order structure in the HA at  
 260 the center of these complexes, even if aggrecan binding alone does not, as it has been suggested that link protein induces  
 261 cooperativity in aggrecan G1 binding (13).

## 262 CONCLUSION

263 We establish low-force stretching as a useful technique to detect and study proteoglycan binding to HA. Side chain induced  
 264 swelling affects HA's chain structure on long length-scales: 10s to 100s of nm. Structure on these scales is sensitive to  
 265 sub-picowatt forces, accessible using magnetic tweezers. Here, we have used this technique to quantify the expansion  
 266 undergone by a single HA chain at the center of an HA-aggrecan bottlebrush complex (see Fig. 2), and found that inter-aggrecan  
 267 repulsion generates an internal tension of about 0.5 pN. We have also examined the complexes under larger stretching forces  
 268 ( $\sim 1$ -10 pN) where all long length-scale structure has been pulled out and we are sensitive to small structures ( $\sim$ nm). At these  
 269 high forces (short length-scales), we find no difference in HA chain structure with and without aggrecan, indicating that while  
 270 aggrecan causes significant swelling of the random coil structure of HA, its binding does not cause any local structure changes.

271 While all experiments show swelling, we observe significant variability in the force-response of the aggrecan-decorated HA  
 272 chains, which is likely caused by polydispersity of the aggrecan. We use a theory of bottlebrush polymers with previously  
 273 measured physical parameters for aggrecan, and find that our data are bounded by the expected limits for fully glycosylated and  
 274 deglycosylated aggrecan. In doing so, we demonstrate the sensitivity of the magnetic tweezers technique to the molecular level  
 275 degradation of proteoglycans, and connect the chemistry of aggrecan to the mechanics of larger-scale structures in cartilage.

276 Our experimentally validated model quantitatively predicts how bottlebrush architecture leads to the expanded nature of the  
 277 HA-aggrecan complex, which is crucial in maintaining the structural integrity of cartilage. While swelling is expected from  
 278 previous work (33, 34), developing a firm physical basis for the system improves understanding of the basic processes, and offers  
 279 quantitative methods that can later be extended to answer other biological questions. Aggrecan glycosylation undergoes slight  
 280 changes with age, but the more dramatic alterations to aggrecan structure occur in pathologic conditions, where aggrecanase  
 281 enzymes cleave the core protein, at times removing some or all of the CS-attachment domain (9, 10). The model presented  
 282 here makes predictions for how the complex structure will change in the case of reduced core protein size; future work will  
 283 explore aggrecan proteolysis and evaluate these predictions. Further, the internal tension/brush model will likely be useful to  
 284 describe complexes of HA with other proteoglycans (e.g. versican and brevican), which have a similar bottlebrush geometry, but  
 285 drastically different biological functions. In these various complexes, changes in the bottlebrush structure will set the tension;  
 286 this in turn will affect not only the extracellular matrix mechanics, but also the force signals transmitted from the exterior to the  
 287 interior of cells, by means of the mechanosensitive HA receptor CD44 (50).

## 288 AUTHOR CONTRIBUTIONS

289 O.A.S., J.P.B., and S.I.-G. designed the research. S.I.-G. and J.P.B. designed and performed experiments, and analyzed data.  
 290 S.I.-G., J.P.B., and O.A.S. wrote the article.

## 291 SUPPORTING MATERIAL

292 An online supplement to this article can be found at [ADDRESS].

293  
 294 This work was supported by the National Science Foundation under grants no. 1611497 and no. 2005189. S.I.-G. thanks Connie  
 295 Frank for fellowship support.

## 296 REFERENCES

- 297 1. Kiani, C., C. Liwen, Y. J. Wu, J. Y. Albert, and B. Y. Burton, 2002. Structure and function of aggrecan. *Cell Research* 12:19.
- 299 2. Cowman, M. K., C. Spagnoli, D. Kudasheva, M. Li, A. Dyal, S. Kanai, and E. A. Balazs, 2005. Extended, relaxed, and  
 300 condensed conformations of hyaluronan observed by atomic force microscopy. *Biophysical Journal* 88:590–602.
- 301 3. Bastow, E. R., S. Byers, S. B. Golub, C. E. Clarkin, A. A. Pitsillides, and A. J. Fosang, 2008. Hyaluronan synthesis and  
 302 degradation in cartilage and bone. *Cellular and Molecular Life Sciences* 65:395–413.
- 303 4. Knudson, C. B., and W. Knudson, 2001. Cartilage proteoglycans. In *Seminars in cell & developmental biology*. Elsevier,  
 304 volume 12, 69–78.
- 305 5. Lee, H.-Y., L. Han, P. J. Roughley, A. J. Grodzinsky, and C. Ortiz, 2013. Age-related nanostructural and nanomechanical  
 306 changes of individual human cartilage aggrecan monomers and their glycosaminoglycan side chains. *Journal of Structural  
 307 Biology* 181:264–273.
- 308 6. Vasan, N., 1980. Proteoglycans in normal and severely osteoarthritic human cartilage. *Biochemical Journal* 187:781–787.
- 309 7. Watanabe, H., Y. Yamada, and K. Kimata, 1998. Roles of aggrecan, a large chondroitin sulfate proteoglycan, in cartilage  
 310 structure and function. *The journal of biochemistry* 124:687–693.
- 311 8. Hardingham, T., 1998. Chondroitin sulfate and joint disease. *Osteoarthritis and cartilage* 6:3–5.
- 312 9. Duhdia, J., 2005. Aggrecan, aging and assembly in articular cartilage. *Cellular and Molecular Life Sciences CMLS*  
 313 62:2241–2256.

314 10. Ng, L., A. J. Grodzinsky, P. Patwari, J. Sandy, A. Plaas, and C. Ortiz, 2003. Individual cartilage aggrecan macromolecules  
315 and their constituent glycosaminoglycans visualized via atomic force microscopy. *Journal of Structural Biology* 143:242 –  
316 257.

317 11. Mörgelin, M., M. Paulsson, T. Hardingham, D. Heinegård, and J. Engel, 1988. Cartilage proteoglycans. Assembly with  
318 hyaluronate and link protein as studied by electron microscopy. *Biochemical Journal* 253:175–185.

319 12. Mörgelin, M., M. Paulsson, D. Heinegård, U. Aebi, and J. Engel, 1995. Evidence of a defined spatial arrangement of  
320 hyaluronate in the central filament of cartilage proteoglycan aggregates. *Biochemical Journal* 307:595–601.

321 13. Neame, P., and F. Barry, 1993. The link proteins. *Experientia* 49:393–402.

322 14. Yeh, M.-L., and Z.-P. Luo, 2004. The structure of proteoglycan aggregate determined by atomic force microscopy. *Scanning: The Journal of Scanning Microscopies* 26:273–276.

324 15. Harder, A., V. Walhorn, T. Dierks, X. Fernández-Busquets, and D. Anselmetti, 2010. Single-Molecule Force Spectroscopy  
325 of Cartilage Aggrecan Self-Adhesion. *Biophysical Journal* 99:3498 – 3504.

326 16. Han, L., D. Dean, P. Mao, C. Ortiz, and A. J. Grodzinsky, 2007. Nanoscale Shear Deformation Mechanisms of Opposing  
327 Cartilage Aggrecan Macromolecules. *Biophysical Journal* 93:L23 – L25.

328 17. Neuman, K. C., and A. Nagy, 2008. Single-molecule force spectroscopy: optical tweezers, magnetic tweezers and atomic  
329 force microscopy. *Nature methods* 5:491.

330 18. Saleh, O. A., 2015. Perspective: Single polymer mechanics across the force regimes. *The Journal of chemical physics*  
331 142:194902.

332 19. Fantner, G. E., E. Oroudjev, G. Schitter, L. S. Golde, P. Thurner, M. M. Finch, P. Turner, T. Gutsmann, D. E. Morse,  
333 H. Hansma, and P. K. Hansma, 2006. Sacrificial Bonds and Hidden Length: Unraveling Molecular Mesostructures in  
334 Tough Materials. *Biophysical Journal* 90:1411 – 1418.

335 20. Kienle, S., M. Gallei, H. Yu, B. Zhang, S. Krysiak, B. N. Balzer, M. Rehahn, A. D. Schlüter, and T. Hugel, 2014. Effect of  
336 Molecular Architecture on Single Polymer Adhesion. *Langmuir* 30:4351–4357. PMID: 24679005.

337 21. Liu, X., J. Q. Sun, M. H. Heggeness, M.-L. Yeh, and Z.-P. Luo, 2004. Direct quantification of the rupture force of single  
338 hyaluronan/hyaluronan binding protein bonds. *FEBS letters* 563:23–27.

339 22. Bano, F., M. I. Tammi, D. W. Kang, E. N. Harris, and R. P. Richter, 2018. Single-molecule unbinding forces between the  
340 polysaccharide hyaluronan and its binding proteins. *Biophysical journal* 114:2910–2922.

341 23. Liu, X., P. C. Noble, and Z.-P. Luo, 2003. A method for testing compressive properties of single proteoglycan aggregates.  
342 *Biochemical and biophysical research communications* 307:338–341.

343 24. Liu, X., P. C. Noble, and Z.-P. Luo, 2004. Direct measurements of the compressive properties of single proteoglycan  
344 aggregates. *Biochemical and biophysical research communications* 316:313–316.

345 25. Wang, Y., L. M. McNamara, M. B. Schaffler, and S. Weinbaum, 2007. A model for the role of integrins in flow induced  
346 mechanotransduction in osteocytes. *Proceedings of the National Academy of Sciences* 104:15941–15946.

347 26. Jacobson, D. R., D. B. McIntosh, M. J. Stevens, M. Rubinstein, and O. A. Saleh, 2017. Single-stranded nucleic acid  
348 elasticity arises from internal electrostatic tension. *Proceedings of the National Academy of Sciences* 114:5095–5100.

349 27. Pincus, P., 1976. Excluded volume effects and stretched polymer chains. *Macromolecules* 9:386–388.

350 28. Berezney, J. P., A. B. Marciel, C. M. Schroeder, and O. A. Saleh, 2017. Scale-dependent stiffness and internal tension of a  
351 model brush polymer. *Physical review letters* 119:127801.

352 29. Strick, T. R., J.-F. Allemand, D. Bensimon, V. Croquette, 1998. Behavior of Supercoiled DNA. *Biophysical Journal*  
353 74:2016–2028.

354 30. Han, L., D. Dean, L. A. Daher, A. J. Grodzinsky, and C. Ortiz, 2008. Cartilage Aggrecan Can Undergo Self-Adhesion.  
355 *Biophysical Journal* 95:4862–4870.

356 31. Ribeck, N., and O. A. Saleh, 2008. Multiplexed single-molecule measurements with magnetic tweezers. *Review of Scientific*  
 357 *Instruments* 79:094301.

358 32. Lansdorp, B. M., and O. A. Saleh, 2012. Power spectrum and Allan variance methods for calibrating single-molecule  
 359 video-tracking instruments. *Review of Scientific Instruments* 83:025115.

360 33. Chang, P. S., L. T. McLane, R. Fogg, J. Scrimgeour, J. S. Temenoff, A. Granqvist, and J. E. Curtis, 2016. Cell surface  
 361 access is modulated by tethered bottlebrush proteoglycans. *Biophysical Journal* 110:2739–2750.

362 34. Attili, S. and R. P. Richter, 2013. Self-assembly and elasticity of hierarchical proteoglycan-hyaluronan brushes. *Soft Matter*  
 363 9:10473–10483.

364 35. Papagiannopoulos, A., T. Waigh, T. Hardingham, and M. Heinrich, 2006. Solution structure and dynamics of cartilage  
 365 aggrecan. *Biomacromolecules* 7:2162–2172.

366 36. Nap, R. J., and I. Szleifer, 2008. Structure and Interactions of Aggrecans: Statistical Thermodynamic Approach. *Biophysical*  
 367 *Journal* 95:4570 – 4583.

368 37. Marko, J. F., and E. D. Siggia, 1995. Statistical mechanics of supercoiled DNA. *Phys. Rev. E* 52:2912–2938.

369 38. Matthews, R. T., G. M. Kelly, C. A. Zerillo, G. Gray, M. Tiemeyer, and S. Hockfield, 2002. Aggrecan Glycoforms  
 370 Contribute to the Molecular Heterogeneity of Perineuronal Nets. *Journal of Neuroscience* 22:7536–7547.

371 39. Lee, H.-Y., P. Kopesky, A. Plaas, J. Sandy, J. Kisiday, D. Frisbie, A. Grodzinsky, and C. Ortiz, 2010. Adult bone marrow  
 372 stromal cell-based tissue-engineered aggrecan exhibits ultrastructure and nanomechanical properties superior to native  
 373 cartilage. *Osteoarthritis and cartilage* 18:1477–1486.

374 40. Panyukov, S., E. B. Zhulina, S. S. Sheiko, G. C. Randall, J. Brock, and M. Rubinstein, 2009. Tension amplification in  
 375 molecular brushes in solutions and on substrates. *The Journal of Physical Chemistry B* 113:3750–3768.

376 41. Birshtein, T., O. Borisov, Y. Zhulina, A. Khokhlov, and T. Yurasova, 1987. Conformations of comb-like macromolecules.  
 377 *Polymer Science U.S.S.R.* 29:1293 – 1300.

378 42. Jowitt, T. A., A. D. Murdoch, C. Baldock, R. Berry, J. M. Day, and T. E. Hardingham, 2010. Order within disorder:  
 379 Aggrecan chondroitin sulphate-attachment region provides new structural insights into protein sequences classified as  
 380 disordered. *Proteins: Structure, Function, and Bioinformatics* 78:3317–3327.

381 43. Rosales, A. M., H. K. Murnen, S. R. Kline, R. N. Zuckermann, and R. A. Segalman, 2012. Determination of the persistence  
 382 length of helical and non-helical polypeptoids in solution. *Soft Matter* 8:3673–3680.

383 44. Marsh, J. A., and J. D. Forman-Kay, 2010. Sequence determinants of compaction in intrinsically disordered proteins.  
 384 *Biophysical journal* 98:2383–2390.

385 45. Seyfried, N. T., A. J. Day, and A. Almond, 2006. Experimental evidence for all-or-none cooperative interactions between  
 386 the G1-domain of versican and multivalent hyaluronan oligosaccharides. *Matrix biology: journal of the International*  
 387 *Society for Matrix Biology* 25:14.

388 46. Hardingham, T. E., and H. Muir, 1973. Binding of oligosaccharides of hyaluronic acid to proteoglycans (Short  
 389 Communication). *Biochemical Journal* 135:905–908.

390 47. Kulić, I. M., H. Mohrbach, V. Lobaskin, R. Thaokar, and H. Schiessel, 2005. Apparent persistence length renormalization  
 391 of bent DNA. *Phys. Rev. E* 72:041905.

392 48. Dobrynin, A. V., J.-M. Y. Carrillo, and M. Rubinstein, 2010. Chains Are More Flexible Under Tension. *Macromolecules*  
 393 43:9181–9190.

394 49. Foulcer, S., 2012. Structural and Functional Studies on the G1 Domain of Human Versican. Ph.D. thesis, The University of  
 395 Manchester (United Kingdom).

396 50. Kim, Y., and S. Kumar, 2014. CD44-mediated adhesion to hyaluronic acid contributes to mechanosensing and invasive  
 397 motility. *Molecular Cancer Research* 12:1416–1429.